J|A|C|S ARTICLES

Published on Web 06/02/2010

Organic n-Channel Field-Effect Transistors Based on Arylenediimide-Thiophene Derivatives

Rocío Ponce Ortiz,[†,‡] Helena Herrera,[§] Raúl Blanco,[§] Hui Huang,[†] Antonio Facchetti,*[,†,||] Tobin J. Marks,*[,†] Yan Zheng,[||] and José L. Segura*[,§]

Department of Chemistry and the Materials Research Center, Northwestern University, 2145 Sheridan Road, Evanston, Illinois 60208, Department of Physical Chemistry, University of Málaga, Malaga 29071, Spain, Department of Organic Chemistry, Complutense University of Madrid, Faculty of Chemistry, Madrid 28040, Spain, and Polyera Corporation, 8045 Lamon Avenue, Skokie, Illinois 60077

Received March 11, 2010; E-mail: a-facchetti@northwestern.edu; t-marks@northwestern.edu; segura@quim.ucm.es

Abstract: The synthesis, structural, electrochemical, and thin film electrical and electronic structural properties of a series of arylene diimide-oligothiophene n-type semiconductors are reported. This family of compounds allows analysis of the effects on thin film transistor performance of the following: (i) oligothiophene backbone catenation; (ii) naphthalenediimide vs perylenediimide core interchange; (iii) phenylene group introduction in the oligothiophene backbone. Electrochemical experiments indicate similar redox energetics for all members of this series, while thin film transistor measurements reveal markedly different charge transport performances. The highest electron mobility of 0.35 $cm^2 V^{-1} s^{-1}$ is recorded for films of benzo[*lmn*]thieno[3′,4′:4,5]imidazo[2,1-*b*][3,8]phenanthroline-1,3,6(2*H*)-trione, 2-octyl (**NDI-1T**). Solution-processed field effect transistors were also fabricated and surprisingly exhibit electrical performances surpassing that of the vapor-deposited films in the case of isoquino[6′,5′,4′:10,5,6]anthra[2,1,9-*def*]thieno[3′,4′:4,5]imidazo[2,1-*a*]isoquinoline-1,3,8(2*H*)-trione, 2-(1-heptyloctyl)-10,12-di-2-thienyl (**PDI-3T**).

Introduction

In the field of organic electronics, both n- and p-type semiconductors are required to fabricate complementary logic circuits.[1] To date, p-type materials with mobilities comparable to, or even surpassing, that of amorphous silicon in performance, such as pentacene, rubrene, etc., have been successfully realized.[2] In contrast, n-type organic materials suitable to replace n-type inorganic electronic materials still present challenges.[3,4] In fact, the most studied n-type organic semiconductors typically lack air stability, and their mobilities tend to be an order of magnitude smaller than those of the corresponding p-type homologues.[5] One successful strategy used to achieve and enhance electron conduction and carrier stability in organic semiconductors has involved the treatment of the most common SiO_2 gate dielectric with organic monolayers to remove Si−OH groups on the surface that act as trap sites[6] and to modulate the semiconductor growth and microstructure.[7] Another strategy has been to select contact metals with low workfunctions, able to efficiently inject electrons into the LUMOs of electron-deficient organic semiconductors.[8] However, while these strategies, among others,[9] have enhanced the electron mobility of some n-type semiconductor classes, it has usually been at the expense of air stability. For these reasons, creating and learning to manipulate the properties of new n-type materials[10] are essential to fully understand electron conduction mechanisms and to achieve the stability and processability goals imposed by the new organic electronics era. Imide-substituted perylene and naphthalene derivatives have proven to be interesting candidates

[†] Northwestern University.
[‡] University of Málaga.
[§] Complutense University of Madrid.
[||] Polyera Corporation.

(1) Klauk, H.; Zschieschang, U.; Pflaum, J.; Halik, M. *Nature* **2007**, *445*, 745.
(2) (a) Sundar, V. C.; Zaumseil, J.; Podzorov, V.; Menard, E.; Willett, R. L.; Someya, T.; Gershenson, M. E.; Rogers, J. A. *Science* **2004**, *303*, 1644. (b) Halik, M.; Klauk, H.; Zschieschang, U.; Schmid, G.; Dehm, C.; Schütz, M.; Maisch, S.; Effenberger, F.; Brunnbauer, M.; Stellacci, F. *Nature* **2004**, *431*, 963. (c) Dimitrakopoulos, C. D.; Purushothaman, S.; Kymissis, J.; Callegari, A.; Shaw, J. M. *Science* **1999**, *283*, 822. (d) Nelson, S. F.; Lin, Y.-Y.; Gundlach, D. J.; Jackson, T. N. *Appl. Phys. Lett.* **1998**, *72*, 1854.
(3) Newman, C. R.; Frisbie, C. D.; da Silva Filho, D. A.; Brèdas, J. L.; Ewbank, P. C.; Mann, K. R. *Chem. Mater.* **2004**, *16*, 4436.
(4) Dimitrakoupoulos, C. D.; Mascaro, D. J. *IBM J. Res. Dev.* **2001**, 45.
(5) Facchetti, A. *Mater. Today* **2007**, *10*, 28.
(6) Chua, L. L.; Zaumseil, J.; Chang, J. F.; Ou, E. C. W.; Ho, P. K. H.; Sirringhaus, H. R.; Friend, H. *Nature* **2005**, *434*, 194.
(7) Dhagat, P.; Haverinen, H. M.; Kline, R. J.; Jung, Y.; Fischer, D. A.; DeLongchamp, D. M.; Jabbour, G. E. *Adv. Funct. Mater.* **2009**, *19*, 2365.
(8) (a) Kobayashi, S.; Takenobu, T.; Mori, S.; Fujiwara, A.; Iwasa, Y. *Appl. Phys. Lett.* **2003**, *82*, 4581. (b) Haddon, R. C.; Perel, A. S.; Morris, R. C.; Palstra, T. T. M.; Hebard, A. F.; Fleming, R. M. *Appl. Phys. Lett.* **1995**, *67*, 121.
(9) Nakayama, K.-I.; Ishikawa, M.; Yokoyama, M. *Appl. Phys. Express* **2009**, *2*, 021501.
(10) (a) Tang, M. L.; Oh, J. H.; Reichard, A. D.; Bao, Z. *J. Am. Chem. Soc.* **2009**, *131*, 3733. (b) Ruiz Delgado, M. C.; Pigg, K. R.; da Silva Filho, D. A.; Gruhn, N. E.; Sakamoto, Y.; Suzuki, T.; Malavé Osuna, R.; Casado, J.; Hernández, V.; López Navarrete, J. T.; Martinelli, N. G.; Cornil, J.; Sánchez Carrera, R. S.; Coropceanu, V.; Bredas, J. L. *J. Am. Chem. Soc.* **2009**, *131*, 1502. (c) Ruiz Delgado, M. C.; Kim, E.-G.; da Silva, D. A.; Bredas, J. L. *J. Am. Chem. Soc.* **2010**, *132*, 3375.

 10.1021/ja1018783

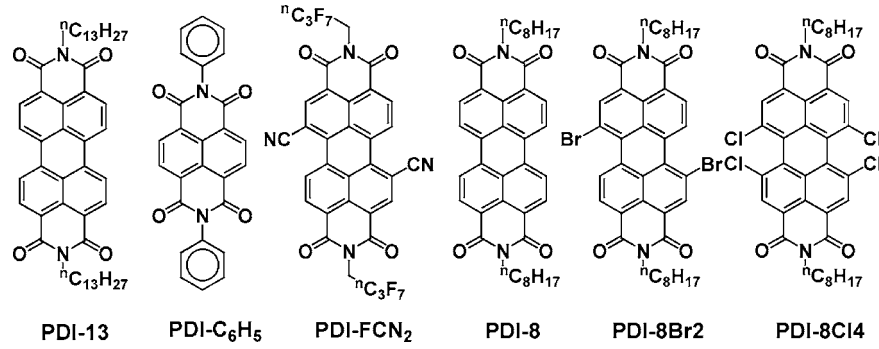

Figure 1. Chemical structures of some n-type arylenediimide semiconductors.

for electron transport in a variety of device architectures,[11,12] and substantial electron mobilities (>0.1 $cm^2\ V^{-1}\ s^{-1}$) have been reported for TFTs fabricated/characterized under ambient conditions.[13−16] In perylene derivatives, the device performance in vacuum has been shown to be sensitive to the nature of the alkyl substituents[17] and film thermal annealing,[18] with mobilities as high as 2.1 $cm^2\ V^{-1}\ s^{-1}$ reported for a *N*,*N*′-ditridecyl-3,4,9,10-perylenetetracarboxylic diimide (**PDI-13**, Figure 1) semiconductor annealed at 140 °C.[18] Recently, a field-effect mobility approaching 6 $cm^2\ V^{-1}\ s^{-1}$ has been claimed for a *N*,*N*′-bis(cyclohexyl)naphthalene diimide (**PDI-C_6H_5**, Figure 1) semiconductor measured under a continuous stream of argon at 22% relative humidity.[19] Under ambient conditions, a mobility of 0.64 $cm^2\ V^{-1}\ s^{-1}$ was reported by Jones et al. for an *N*-fluoroalkyl core-cyanated perylene derivative (**PDI-FCN_2**, Figure 1).[13]

In PDI-based materials with *N*-fluoroalkyl substitution, stability in air is found to be dependent on the fluorination level and fluorine substitution pattern[20,21] and has been ascribed by some researchers to the presence of the larger fluorine atoms instead of smaller hydrogen atoms in the substituent *N*-alkyl chains. Katz et al. proposed that the larger fluorine van der Waals radius relative to hydrogen leads to decreased free volume between packed alkyl chains (from ∼4 Å to ∼2 Å), hindering O_2 difusion.[22] Another hypothesis, first advanced by de Leeuw et al., is that the stability of the charge carriers with respect to H_2O and O_2 depends on the redox potential of the organic semiconductor.[23] In this regard, Jones et al. reported that, for a family of arylenediimide semiconductors, air-stable n-type mobility with minimal hysteresis was observed whenever the reduction potential was more positive than −0.1 V.[13c] However, Weitz et al. studied n-channel transistors based on core-cyanated perylene carboxylic diimide derivatives with different *N*-fluoroalkyl substituents and claimed that a mechanism unrelated to either the redox potential or the presence of a kinetic barrier was responsible for the air stability.[24] These results make clear that additional research is required to fully understand organic electron charge transport mechanisms and trapping in such materials.

Oligothiophenes substituted with electron-withdrawing groups such as fluoro-alkyl chains[25] or cyano groups (leading to quinoidal[26,27] or cross-conjugated structures[28]) have also been found to exhibit substantial n-type mobilities[25,26] and even ambipolar[27,28] (hole and electron) conduction. Ambipolar semiconductors can also be used for the fabrication of comple-

(11) (a) Tang, C. W. *Appl. Phys. Lett.* **1986**, *48*, 183. (b) Forrest, S. R. *Chem. Rev.* **1997**, *97*, 1793.
(12) (a) Dittmer, J. J.; Marseglia, E. A.; Friend, R. H. *Adv. Mater.* **2000**, *12*, 1270. (b) Schmidt-Mende, L.; Fechtenkötter, A.; Müllen, K.; Moons, E.; Friend, R. H.; Mackenzie, J. D. *Science* **2001**, *293*, 1119.
(13) (a) Jones, B. A.; Facchetti, A.; Wasielewski, M. R.; Marks, T. J. *Adv. Funct. Mater.* **2008**, *18*, 1329. (b) Jones, B. A.; Facchetti, A.; Marks, T. J.; Wasielewski, M. R. *Chem. Mater.* **2007**, *19*, 2703. (c) Jones, B. A.; Facchetti, A.; Wasielewski, M. R.; Marks, T. J. *J. Am. Chem. Soc.* **2007**, *129*, 15259. (d) Jung, T.; Yoo, B.; Wang, L.; Dodabalapur, A.; Jones, B. A.; Facchetti, A.; Wasielewski, M. R.; Marks, T. J. *Appl. Phys. Lett.* **2006**, *88*, 183102. (e) Jones, B. A.; Ahrens, M. J.; Yoon, M.-H.; Facchetti, A.; Marks, T. J.; Wasielewski, M. R. *Angew. Chem., Int. Ed.* **2004**, *43*, 6363.
(14) (a) Schmidt, R.; Oh, J. H.; Sun, Y.-S.; Deppisch, M.; Krause, A.-M.; Radacki, K.; Braunschweig, H.; Könemann, M.; Erk, P.; Bao, Z.; Würthner, F. *J. Am. Chem. Soc.* **2009**, *131*, 6215. (b) Ling, M.; Erk, P.; Gomez, M.; Koenemann, M.; Locklin, J.; Bao, Z. *Adv. Mater.* **2007**, *19*, 1123.
(15) Schmidt, R.; Ling, M. M.; Oh, J. H.; Winkler, M.; Könemann, M.; Bao, Z.; Würthner, F. *Adv. Mater.* **2007**, *19*, 3692.
(16) See, K. C.; Landis, C.; Sarjeant, A.; Katz, H. E. *Chem. Mater.* **2008**, *20*, 3609.
(17) (a) Chesterfield, R. J.; McKeen, J. C.; Newman, C. R.; Frisbie, C. D.; Ewbank, P. C.; Mann, K. R.; Miller, L. L. *J. Appl. Phys.* **2004**, *95*, 6396. (b) Chesterfield, R. J.; McKeen, J. C.; Newman, C. R.; Ewbank, P. C.; da Silva Filho, D. A.; Brèdas, J.-L.; Miller, L. L.; Mann, K. R.; Frisbie, C. D. *J. Phys. Chem. B* **2004**, *108*, 19281. (c) Malenfant, P. R. L.; Dimitrakopoulos, C. D.; Gelorme, J. D.; Kosbar, L. L.; Graham, T. O.; Curioni, A.; Andreoni, W. *Appl. Phys. Lett.* **2002**, *80*, 2517. (d) Zschieschang, U.; Amsharov, K.; Weitz, R. T.; Jansen, M.; Klauk, H. *Synth. Met.* **2009**, *159*, 2362.
(18) Tatemichi, S.; Ichikawa, M.; Koyama, T.; Taniguchi, Y. *Appl. Phys. Lett.* **2006**, *89*, 112108.
(19) Shukla, D.; Nelson, S. F.; Freeman, D. C.; Rajeswaran, M.; Ahearn, W. G.; Meyer, D. M.; Carey, J. T. *Chem. Mater.* **2008**, *20*, 7486.
(20) (a) Chen, H. A.; Ling, M. M.; Mo, X.; Shi, M. M.; Wang, M.; Bao, Z. *Chem. Mater.* **2007**, *19*, 816. (b) Hosoi, Y.; Tsunami, D.; Ishii, H.; Furukawa, Y. *Chem. Phys. Lett.* **2007**, *436*, 139.
(21) Li, Y.; Tan, L.; Wang, Z.; Qian, H.; Shi, Y.; Hu, W. *Org. Lett.* **2008**, *10*, 529.
(22) (a) Katz, H. E.; Lovinger, A. J.; Johnson, J.; Kloc, C.; Seigrist, T.; Li, W.; Lin, Y.-Y.; Dodabalapur, A. *Nature* **2000**, *404*, 478. (b) Katz, H. E.; Johnson, J.; Lovinger, A. J.; Li, W. *J. Am. Chem. Soc.* **2000**, *122*, 7787.
(23) de Leeuw, D. M.; Simenon, M. M. J.; Brown, A. R.; Einerhand, R. E. F. *Synth. Met.* **1997**, *87*, 53.
(24) Weitz, R. T.; Amsharov, K.; Zschieschang, U.; Barrena Villas, E.; Goswami, D. K.; Burghard, M.; Dösch, H.; Jansen, M.; Kern, K.; Klauk, H. *J. Am. Chem. Soc.* **2008**, *130*, 4637.
(25) (a) Facchetti, A.; Mushrush, M.; Yoon, M.-H.; Hutchison, G. R.; Ratner, M. A.; Marks, T. J. *J. Am. Chem. Soc.* **2004**, *126*, 13859. (b) Facchetti, A.; Yoon, M.-H.; Stern, C. L.; Hutchison, G. R.; Ratner, M. A.; Marks, T. J. *J. Am. Chem. Soc.* **2004**, *126*, 13480. (c) Facchetti, A.; Yoon, M.-H.; Stern, C. L.; Katz, H. E.; Marks, T. J. *Angew. Chem., Int. Ed.* **2003**, *42*, 3900.
(26) Pappenfus, T. M.; Chesterfield, R. J.; Frisbie, C. D.; Mann, K. R.; Casado, J.; Raff, J. D.; Miller, L. L. *J. Am. Chem. Soc.* **2002**, *124*, 4184.
(27) Chesterfield, R. J.; Newman, C. R.; Pappenfus, T. M.; Ewbank, P. C.; Haukaas, M. H.; Mann, K. R.; Miller, L. L.; Frisbie, C. D. *Adv. Mater.* **2003**, *15*, 1278.
(28) Ponce Ortiz, R.; Facchetti, A.; Marks, T. J.; Casado, J.; Zgierski, M. Z.; Kozaki, M.; Hernández, V.; López Navarrete, J. T. *Adv. Funct. Mater.* **2009**, *19*, 386.

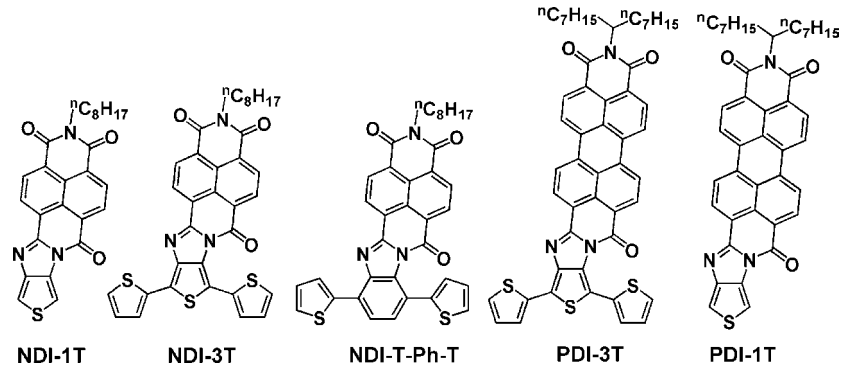

Figure 2. Chemical structures of the compounds in this study.

mentary circuits.[29] One intriguing strategy to combine both ambipolarity and air stability would be to combine arylenediimide skeletons and thiophene rings within the same molecular structure.[30,31] To this end, the first family of molecules consisting of β-naphthalenediimide and β-perylenediimide oligothiophenes was recently synthesized and reported by several of us.[32] Amphoteric redox behavior was established in these molecules by cyclic voltammetry, indicating the possibility of both electron extraction and injection from/into the conjugated π-system. However, the carrier transport properties of these interesting molecules as thin films remained unknown. This contribution focuses on extending this semiconductor family and targets the fabrication and characterization of organic thin film transistors (OTFTs) using the materials depicted in Figure 2 as the semiconductors. It will be seen that electron transport is facile for all of these materials while hole transport is hindered, probably reflecting oligothiophene skeletal distorsions, which disrupt π-conjugation.

The present family of compounds allows analysis of the interplay of three very different effects on OTFT device response characteristics: (i) oligothiophene backbone catenation by comparing the behavior of **NDI-1T** vs **NDI-3T** and **PDI-1T** vs **PDI-3T**; (ii) interchanging naphthalenediimide and perylenediimide fragments by comparing **NDI-1T** vs **PDI-1T** and **NDI-3T** vs **PDI-3T**, and finally (iii) introducing a phenylene fragment into the oligothiophene backbone by the analysis of **NDI-T-Ph-T**.[32] Furthermore, for large scale fabrication of low-cost devices, low-temperature solution-based film deposition processes are highly desirable. For this purpose, the organic semiconductor layer should be deposited using solution-processing techniques such as spin-coating, solution-casting, inkjet printing, etc. that are much simpler and less capital-intensive than those commonly used for conventional inorganic microelectronics.[33,34] Solution-processed field-effect transistors based on other less elaborate arylenediimide semiconductors have already been reported by several groups.[35,36] In the final part of this contribution, solution-processed devices fabricated with several of the present compounds are described and analyzed.

For the same reasons as discussed above, the fabrication of single-crystal devices from solution offers both attractions and challenges. Indeed, several recent reports described using perylenediimide derivatives (e.g., *N*,*N*′-dialkyl substituted perylenediimides with 5−13 carbon alkyl chains) to grow randomly oriented nanowires from solution with mobilities on the order of 10^{-2} cm^2 V^{-1} s^{-1}.[37] Furthermore, alignment of these perylenediimide-based micro- and nanowires afforded electron mobilities up to 0.24 cm^2 V^{-1} s^{-1} for wire networks and electron mobilities as high as 1.4 cm^2 V^{-1} s^{-1} for single microwires.[38]

Results

The synthesis and purification of the semiconductors **NDI-1T**, **NDI-3T**, and **PDI-3T** have been discussed elsewhere.[32] The synthetic procedures for **NDI-T-Ph-T** and **PDI-1T** are shown in Scheme 1 (see the Supporting Information for details). The reagents 3,6-dibromo-1,2-phenylenediamine (**1**),[39] *N*-(*n*-octyl)-naphthalene-1,8-dicarboxyanhydride-4,5-dicarboximide (**2**),[40] 3,4-diaminothiophene (**6**),[41] and *N*-(8-heptadecyl)-3,4,9,10-perylenetetracarboxylic 3,4-anhydride-9,10-imide (**7**)[42] were prepared according to the literature. All other reagents were purchased from Aldrich and used as received without further purification.

(29) (a) Handa, S.; Miyazaki, E.; Takimiya, K. *Chem. Commun.* **2009**, *26*, 3919. (b) Yang, C.-Y.; Dhananjay; Chen, S. S.; Ou, C.-W.; Chuang, Y.-C.; Wu, M.-C.; Chu, C.-W. *Appl. Phys. Lett.* **2008**, *92*, 253307.
(30) You, C.-C.; Saha-Möller, C. R.; Würthner, F. *Chem. Commun.* **2004**, 2030.
(31) Segura, J. L.; Gómez, R.; Blanco, R.; Reinold, E.; Bauerle, P. *Chem. Mater.* **2006**, *18*, 2834.
(32) (a) González, S. R.; Casado, J.; López Navarrete, J. T.; Blanco, R.; Segura, J. L. *J. Phys. Chem. A* **2008**, *112*, 6732. (b) Blanco, R.; Gómez, R.; Seoane, C.; Segura, J. L.; Mena-Osteritz, E.; Bäuerle, P. *Org. Lett.* **2007**, *9*, 2171.
(33) (a) Forrest, S. R. *Nature* **2004**, *428*, 911. (b) Katz, H. *Chem. Mater.* **2004**, *16*, 4748. (c) *Printed Organic and Molecular Electronics*; Gamota, D., Brazis, P., Kalyanasundaram, K., Zhang, J., Eds.; Kluwer Academic Publishers: Boston, 2004.
(34) (a) Kelley, T. W.; Baude, P. F.; Gerlach, C.; Ender, D. E.; Muyres, D.; Haase, M. A.; Vogel, D. E.; Theiss, S. D. *Chem. Mater.* **2004**, *16*, 4413. (b) Sheats, J. R. *J. Mater. Res.* **2004**, *19*, 1974.
(35) (a) Lee, Y.-L.; Hsu, H.-L.; Chen, S.-Y.; Yew, T.-R. *J. Phys. Chem. C* **2008**, *112*, 1694. (b) Singh, Th. B.; Erten, S.; Günes, S.; Zafer, C.; Turkmen, G.; Kuban, B.; Teoman, Y.; Sariciftci, N. S.; Icli, S. *Org. Electron.* **2006**, *7*, 480.
(36) (a) Piliego, C.; Cordella, F.; Jarzab, D.; Lu, S.; Chen, Z.; Facchetti, A.; Loi, M. A. *Appl. Phys. A: Mater. Sci. Process.* **2009**, *95*, 303. (b) Yan, H.; Zhen, Y.; Blache, R.; Newman, C.; Lu, S.; Woerle, J.; Facchetti, A. *Adv. Mater.* **2008**, *20*, 3393. (c) Gawrys, P.; Boudinet, D.; Zagorska, M.; Djurado, D.; Verilhac, J.-M.; Horowitz, G.; Pécaud, J.; Pouget, S.; Pron, A. *Synth. Met.* **2009**, *159*, 1478.
(37) Briseno, A. J.; Mannsfeld, S. C. B.; Reese, C.; Hancock, J. M.; Xiong, Y.; Jenekhe, S. A.; Bao, Z.; Xia, Y. *Nano Lett.* **2007**, *7*, 2847.
(38) Oh, J. H.; Lee, H. W.; Mannsfeld, S.; Stoltenberg, R. M.; Jung, E.; Jin, Y. W.; Kim, J. M.; Yoo, J.-B.; Bao, Z. *Proc. Natl. Acad. Sci. U.S.A.* **2009**, *106*, 6065.
(39) Tsubata, Y.; Suzuki, T.; Miyashi, T.; Yamashita, Y. *J. Org. Chem.* **1992**, *57*, 6749.
(40) Greenfield, A. R.; Svec, W. A.; Gosztola, D.; Wasielewski, M. R. *J. Am. Chem. Soc.* **1996**, *118*, 6749.
(41) Kenning, D. D.; Mitchell, K. A.; Calhoun, T. R.; Funfar, M. R.; Sattler, D. J.; Rasmussen, S. C. *J. Org. Chem.* **2002**, *67*, 9073.
(42) Langhals, H.; Sprenger, S.; Brandlherm, M. T. *Liebigs. Ann.* **1995**, 481.

Scheme 1. Synthetic Schemes for **NDI-T-Ph-T** and **PDI-1T**

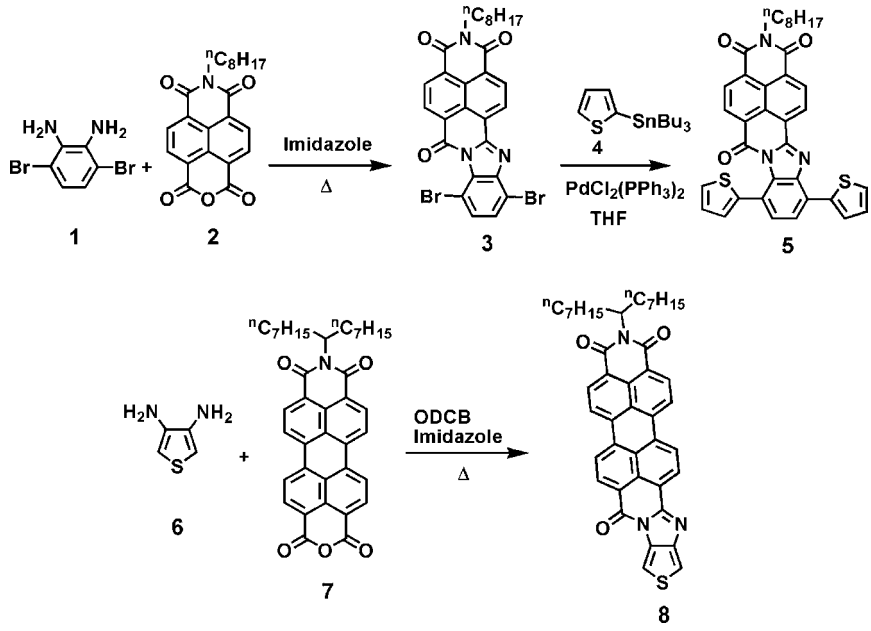

Table 1. Electrochemical Potentials (V) versus SCE of the Indicated Compounds in CH_2Cl_2[a] and Frontier Molecular Orbital Energies Estimated from Cyclic Voltammetry Data

Semiconductor	E_{red1}	E_{red2}	E_{ox1}	E_{ox2}	E_g^{CV}	LUMO[c] (eV)	HOMO[d] (eV)
NDI-1T	−0.65	−1.04	1.39[b]	–	2.04	−3.79	−5.83
NDI-3T	−0.57	−0.93	1.11[b]	–	1.68	−3.87	−5.55
PDI-1T	−0.56	−0.74	1.32[b]	–	1.88	−3.88	−5.76
PDI-3T	−0.55	−0.71	1.06[b]	–	1.61	−3.89	−5.50
NDI-T-Ph-T	−0.57	−0.95	1.42[b]	1.62[b]	1.95	−3.87	−5.82

[a] Referenced to the Fc/Fc^+ couple in CH_2Cl_2 (0.52 V vs SCE). [b] Irreversible. [c] LUMO level estimated vs vacuum level from $E_{LUMO} = -4.44$ eV $- eE_{red1}$. [d] Estimated from HOMO = LUMO[c] $- E_g$. E_g= electrochemical gap.

In the following sections we first discuss the electrochemical characterization of the semiconductors examined in this study, followed by analysis of the thin film microstructural and morphological properties as a function of semiconductor and deposition procedure to understand and optimize TFT device performance. The fabrication and characterization of the devices and comparisons between vapor-deposited and solution-processed devices will be presented next.

Electrochemical Characterization. The electronic properties of the semiconductors in this contribution were characterized by cyclic voltammetry[32] to correlate electronic structure with semiconductor performance. Table 1 summarizes the electrochemical data for the present molecules. The redox potentials were determined as the midpoints between peak potentials for the forward and reverse scans. All the molecules exhibit two reversible reduction processes and one irreversible oxidation wave (two processes are observed for **NDI-T-Ph-T**) within the solvent/electrolyte window range. From these data, the LUMO and HOMO energies were estimated using standard approximations.[43] The energetic positions of the frontier orbital energies are instructive for correlating electronic structure and semiconductor TFT performance. In particular, for organic n-type materials, where charge transport occurs predominantly via hopping through low-lying LUMOs, LUMO energies below −3 eV are usually required for efficient electron injection into the semiconductor from the contacting electrodes.[3,44]

The cyclic voltammetry of **NDI-1T** reveals two reversible reduction processes at −0.65 and −1.04 V. These reduction products are stabilized versus the corresponding reduction products of **NDI** (−0.80 and −1.27 V)[32a] due to the more stable **NDI-1T** LUMO vs that of **NDI**. In good agreement with these results, Gonzalez et al. estimated the B3LYP/6-31G** computed **NDI** LUMO energy to be −3.05 eV vs −3.40 eV for **NDI-1T**.[32a] The introduction of an extended oligothiophene fragment in the structure, namely **NDI-3T**, translates into a slight stabilization of the reduction products (−0.57 and −0.93 V) and significant stabilization of the oxidation product by 0.31 V vs that of **NDI-1T**, resulting in an electrochemical gap reduction from 2.04 to 1.68 eV. This band gap compression is intriguing since the existence of energetically accessible oxidation and reduction products in some cases leads to realization of ambipolar TFT function.[26−28] Another strategy to further compress the electrochemical gap is by substitution of the naphthalene-diimide unit by a perylene-diimide group, as represented by **PDI-1T** and **PDI-3T**. Note that different alkyl substituents are introduced into the two molecules to tune solubility; these modifications should have negligible effects on redox properties. In this case, the first reduction product of the perylenediimide semiconductor is slightly stabilized in the two molecules; however the second product is greatly stabilized (−0.74 and −0.71 V for **PDI-1T** and **PDI-3T**, respectively). In the case of **PDI-3T**, the oxidation potential is shifted to 1.06 V, retaining a band gap of 1.61 V and rendering this value the lowest within the series. Note that the strategy of substituting

(43) (a) Ponce Ortiz, R.; Casado, J.; Hernández, V.; López Navarrete, J. T.; Letizia, J. A.; Ratner, M. A.; Facchetti, A.; Marks, T. J. *Chem.—Eur. J.* **2009**, *15*, 5023. (b) Yoon, M.-H.; DiBenedetto, S. A.; Russel, M. T.; Facchetti, A.; Marks, T. J. *Chem. Mater.* **2007**, *19*, 4864. (c) Dal Colle, M.; Cova, C.; Distefano, G.; Jones, D.; Modelli, A.; Cormisso, N. *J. Phys. Chem. A* **1999**, *103*, 2828.

(44) (a) Hutchison, G. R.; Ratner, M. A.; Marks, T. J. *J. Am. Chem. Soc.* **2005**, *127*, 16866. (b) Hutchison, G. R.; Ratner, M. A.; Marks, T. J. *J. Am. Chem. Soc.* **2005**, *127*, 2339.

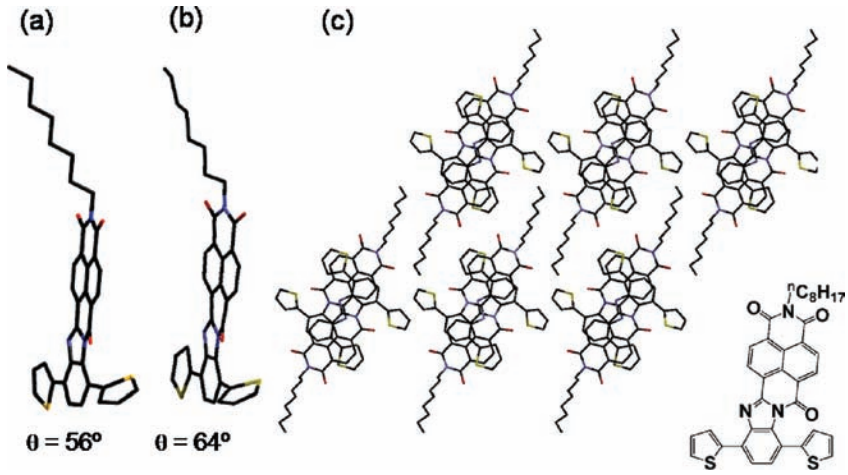

Figure 3. (a) Molecular geometry of **NDI-T-Ph-T** derived from DFT computation. (b) Molecular geometry of **NDI-T-Ph-T** derived from X-ray diffraction analysis. (c) Molecular structure and packing motif of single crystal of **NDI-T-Ph-T**, viewed along the *b*-axis. θ indicates the dihedral angle between the central benzene plane and that of the external twisted thiophene.

the central thiophene ring of **NDI-3T** with a phenylene group, in **NDI-T-Ph-T**, does not significally alter the reduction energetics.

Considering that, in general, incremental electrochemical reduction potential displacement to more positive values correlates with the increasing relative energetic ease of negatively charging the molecular π-system in the solution phase and, thus, the relative stability of the electron charge carriers in the condensed state, one might *a priori* expect a roughly similar OTFT response for all of the present compounds since the first reduction potentials are so similar (Table 1). Nevertheless, other important factors influencing transport properties include internal molecular reorganization accompanying molecular charging[45] and packing modulated $\pi-\pi$ overlap in the solid state.[26]

In contrast to the above considerations for electron transport, the experimental oxidation potentials in Table 1 argue that the hole injection into the semiconductor HOMOs should be facile for the terthiophene derivatives **NDI-3T** and **PDI-3T**, since their HOMO levels are destabilized with respect to **PDI-1T**, **NDI-1T**, and **NDI-T-Ph-T**. Note that replacing the central thiophene ring by a phenylene ring in **NDI-3T** vs **NDI-T-Ph-T** induces a displacement of the first oxidation potential to the same value as that of **NDI-1T**. Nevertheless, a second oxidation process is also observed for **NDI-T-Ph-T** at 1.62 V.

Crystal Structure of NDI-T-Ph-T. Single crystals of the new compound **NDI-T-Ph-T** were grown by slow vapor diffusion of hexane into a dichlorobenzene solution of **NDI-T-Ph-T**, and the crystal structure was determined by X-ray diffraction. The results are shown in Figure 3. The NDI core portion of the molecule adopts a roughly planar configuration. The plane of one thiophene ring is twisted by ~6° with respect to the neighboring aromatic ring plane. In contrast, the second thiophene ring plane is twisted with respect to the phenylene plane by ~64° due to nonbonded repulsive interactions with the keto group.

Furthermore, the arene ring bearing this keto group is also twisted ~17.6° out of the plane of the central aromatic core. Such distorsions arising from intramolecular nonbonded repulsions are common for other **NDI** derivatives which otherwise should have planar structures.[13b,46]

The conjugated **NDI-T-Ph-T** molecules stack along the *b* axis with neighboring molecules packing in a head-to-tail fashion, with partial $\pi-\pi$ overlap at an interplanar separation of 3.28 Å. Self-assembly of the linear alkyl substituent chains affords a lamellar layer structure along the *c* axis. Other molecular metrical parameters are unexceptional for arylenediimides.[13b,46]

Thin Film X-ray Diffraction. Films of the present semiconductors were grown by vacuum sublimation onto Si/SiO_2 substrates. Prior to sublimation, TGA experiments were performed under nitrogen, which indicate partial thermal degradation for **NDI-1T** (34%), **NDI-3T** (48%), and **PDI-3T** (58%) (see Figure S1). The microstructures of the corresponding vapor-deposited thin films were analyzed by means of $\Theta-2\Theta$ diffraction scans. These data quantify microstructural regularity and out-of-plane *d*-spacings, which is essential for estimating molecular orientation with respect to the gate insulator in the case of top-contact devices. It is well-known that the optimal orientation for efficient charge transport between the source and drain electrodes is that in which cofacial π-conjugated planes are aligned perpendicular to the dielectric substrate surface.[47] Furthermore, the appearance of multiple Bragg reflections and Laue oscillations around the first-order Bragg diffraction peak are indications of high semiconductor thin film crystalline quality and of long-range order.[48]

For vapor-phase deposition, the most elaborate diffraction features in the $\Theta-2\Theta$ scans are found for **NDI-1T** at high substrate growth temperatures, 70 and 110 °C. Figure 4 shows **NDI-1T** diffraction data on Si/SiO_2 substrates first treated with either hexamethyldisilazane (HMDS) or octadecyltrichlorosilane (OTS) at 110 °C. A high degree of crystallinity is evidenced from very intense and sharp Bragg reflections. Furthermore, the

(45) Malagoli, M.; Bredas, J. L. *Chem. Phys. Lett.* **2000**, *327*, 13.

(46) (a) Pengo, P.; Dan Pantos, G.; Otto, S.; Sanders, J. K. M. *J. Org. Chem.* **2006**, *71*, 7063. (b) Ofir, Y.; Zelichenok, A.; Yitzchaik, S. *J. Mater. Chem.* **2006**, *16*, 2142. (c) Tomasulo, M.; Naistat, D. M.; White, A. J. P.; Williams, D. J.; Raymo, F. M. *Tetrahedron Lett.* **2005**, *46*, 5695. (d) Dingemans, T. J.; Picken, S. J.; Murthy, N. S.; Mark, P.; StClair, T. L.; Samulski, E. T. *Chem. Mater.* **2004**, *16*, 966.

(47) (a) Sun, Y.; Liu, Y.; Zhu, D. *J. Mater. Chem.* **2005**, *15*, 53. (b) Horowitz, G. *J. Mater. Res.* **2004**, *19*, 1946.

(48) Cullity, B. D.; Stock, S. R. *Elements of X-Ray Diffraction*; Prentice Hall: Upper Saddle River, NJ, 2001.

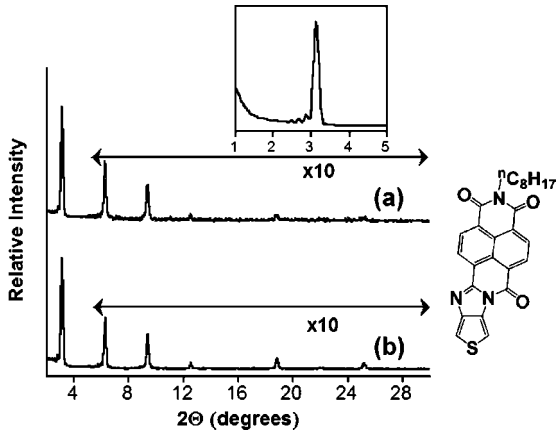

Figure 4. Θ/2Θ X-ray diffraction patterns of **NDI-1T** films deposited at 110 °C on (a) HMDS-treated Si/SiO_2 substrates and (b) OTS-treated Si/SiO_2 substrates. The inset depicts a close-up of the Laue oscillations around the first-order peak for **NDI-1T** deposited on HMDS-treated substrates.

occurrence of (00*l*) progressions is an additional metric of long-range order.[49] Indeed, Bragg reflections up to the eighth order are present for all the **NDI-1T** films, from which a lattice constant of $d \approx 28$ Å is derived. Since single-crystal diffraction data are not available for **NDI-1T**, we assume that the most intense reflection is the first-order (001) reflection and that the remaining peaks are successive reflection orders, as found in similar compounds.[13] Considering the *d*-spacing from these XRD data and the B3LYP/6-31G** computed long axis of the molecule (21.3 Å for **NDI-1T**), the tilt angle with respect to the surface normal can be estimated. Due to the **NDI-1T** molecular dipole moment (0.618 D), it is likely that, similar to **NDI-T-Ph-T** single crystal packing (Figure 3), molecules are packed with pairwise intermolecular interactions orienting the naphthalene-diimide cores in opposite directions, with the long axis of the pairs being ~32.4 Å. Considering this packing motif, the calculated tilt angle should be ~61.2°. In view of the asymmetric structures of the other compounds in the present series, a similar packing motif is expected, and thus, the same approximation is assumed in the following analysis. Note also the appearance of "Laue oscillations" around the first-order Bragg reflection as shown in the inset of Figure 4. These features indicate coherent molecular order across the entire thickness of the deposition.[50]

Figure 5 indicates that **NDI-3T** films deposited at 110 °C on HMDS-treated substrates are essentially amorphous since no Bragg reflections are detected. Previous results of Gonzalez et al.[32a] showed that the optimized molecular geometry of **NDI-3T** exhibits a major increase in the dihedral angle between the thiophene closest to the carbonyl group and the central ring (51.6° vs 17.8° for unsubstituted terthiophene) as in the molecular structure of **NDI-T-Ph-T** (Figure 3), due to non-bonded repulsion between the carbonyl oxygen atom and the thiophene sulfur atom. In contrast, **PDI-1T**, **PDI-3T**, and **NDI-T-Ph-T** films exhibit families of features assignable to (00*l*) reflections and indicating the presence of a single crystalline phase. Nevertheless, the film crystallinity is significantly lower than that in **NDI-1T**, since only two reflections are observed for **PDI-3T** and three for **NDI-T-Ph-T** and **PDI-1T**. For **PDI-3T** films, a similar distortion of the external thiophene ring is expected due to nonbonded repulsions between the carbonyl group of the perylene diimide unit and the sulfur of the aforementioned thiophene ring. Nevertheless, note that **PDI-3T** and **NDI-3T** have very different alkyl chain substituent structures (linear vs branched) and that similar branched alkyl substituents have been used in naphthalene-based polymers exhibiting mobilities of 0.45−0.85 $cm^2\ V^{-1}\ s^{-1}$ for films processed from solution.[51] Thin film diffraction data for the present materials are compiled in Table 2.

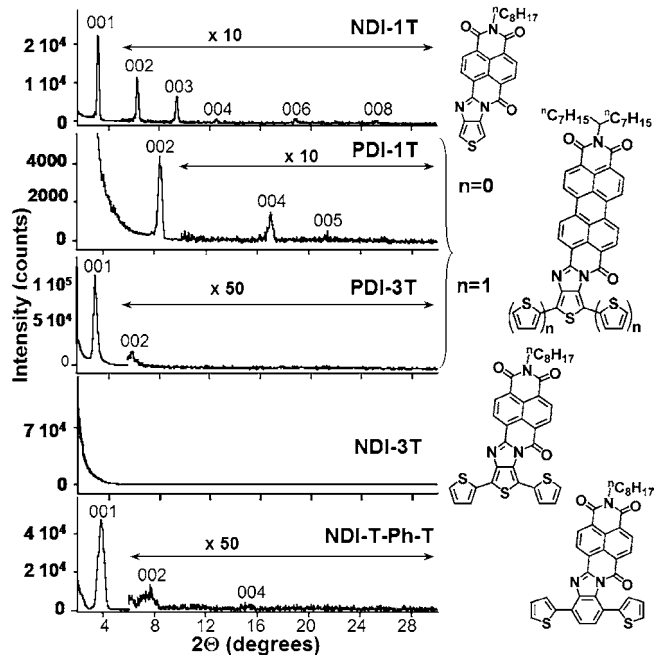

Figure 5. Θ/2Θ X-ray diffraction scans of vapor-deposited **NDI-1T** (T_d = 110 °C), **PDI-1T** (T_d = 110 °C), **PDI-3T** (T_d = 110 °C), **NDI-3T** (T_d = 110 °C) films grown on HMDS-treated Si/SiO_2 and **NDI-T-Ph-T** (T_d = 25 °C) on OTS-treated Si/SiO_2.

Table 2. Thin Film X-ray Diffraction Data for the Various Semiconductors of This Study, Deposited at 110°C onto HMDS-Treated Substrates[a]

Semiconductor	*d*-Spacing (Å)	Molecular Length (Å)	Unit Packing Length (Å)	Tilt Angle (deg)
NDI-1T	28.4	21.3	32.4	61.2
NDI-3T	–	21.3	32.4	–
PDI-1T	20.9	23.7	32.7	39.7
PDI-3T	30.2	24.5	34.4	61.3
NDI-T-Ph-T	22.9	22.2	33.3	43.4

[a] **NDI-T-Ph-T** was deposited at 25°C on OTS-treated substrates. Molecular long axis tilt angles with respect to the surface normal are estimated using experimental *d*-spacings and the unit packing length, where naphthalene/perylene diimide molecular pairs are oriented by intermolecular interactions to face in opposite directions. DFT computed molecular lengths are used to estimate the packing unit dimensions.

Finally, focusing on the room temperature growth of **NDI-T-Ph-T** films on OTS-treated substrates, the observed diffraction pattern (assigned to the (00*l*) progression from the single crystal data) corresponds to a *d*-spacing of ~23 Å (Table 2), which is similar to the *c* cell axis length ~27 Å. This value is significantly smaller than that estimated for **NDI-1T**, even though the theoretical molecular lengths are essentially identical, which

(49) (a) Wie, C. R. *Mater. Sci. Eng., R* **1994**, *R13*, 1. (b) Hadicke, E.; Graser, F. *Acta Crystallogr., Sect. C* **1986**, *42*, 189.
(50) Dürr, A. C.; Schreiber, F.; Münch, M.; Karl, N.; Krause, B.; Kruppa, V.; Dösch, H. *Appl. Phys. Lett.* **2002**, *81*, 2276.
(51) Yan, H.; Chen, Z.; Zheng, Y.; Newman, C.; Quinn, J. R.; Dötz, F.; Kastler, M.; Facchetti, A. *Nature* **2009**, *457*, 679-U1.

Table 3. Thin Film X-ray Diffraction Data for Solution-Processed Thin Films of the Indicated Semiconductors[a]

Semiconductor	*d*-Spacing (Å)	Molecular Length (Å)	Unit Packing Length (Å)	Tilt Angle (deg)
NDI-1T	28.4	21.3	32.4	61.2
NDI-3T	20.8	21.3	32.4	39.9
PDI-1T	31.5	23.7	33.7	69.2
PDI-3T	25.0	24.5	34.4	46.6
NDI-T-Ph-T	18.8	22.2	33.3	34.4

[a] Tilt angles are estimated using experimental *d*-spacings and the computed unit packing length, where two molecules are packed with intermolecular interactions between the two naphthalene/perylene diimide cores facing in opposite directions. DFT theoretical molecular lengths were used to estimate this packing unit length.

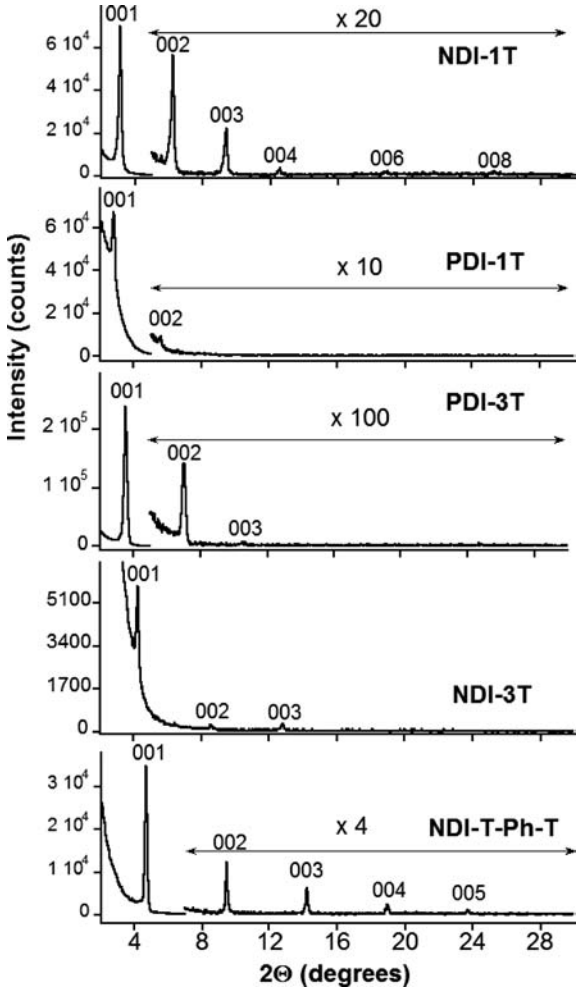

Figure 6. Θ/2Θ X-ray diffraction scans of the indicated solution-proccesed thin films grown on HMDS-treated Si/SiO_2.

suggests a smaller tilt angle (see Table 2). Smaller tilt angles usually correlate with lower mobilities for molecular semiconductors. The same pattern is observed for **PDI-1T** vs **PDI-3T**.

Remarkably, the XRD data for solution-processed thin films of the present materials show comparable or even greater degrees of long-range order than those of vapor-deposited samples (see Table 3 and Figure 6) but, in several cases, significantly different *d*-spacings. This indicates either crystallization of a different phase or a different growth orientation of the same phase. Note also that thermal decomposition is found by TGA in sublimation experiments with **NDI-1T**, **NDI-3T**, and **PDI-3T** (Figure S1). In contrast, **NDI-T-Ph-T** sublimes unchanged, while the crystallinity of the solution-processed films

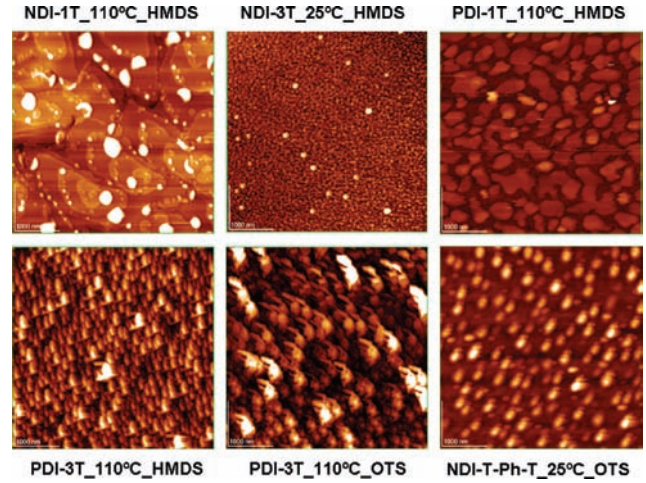

Figure 7. AFM images of the present semiconductors vapor-deposited under conditions yielding optimum TFT performance.

is greater than those grown by sublimation at room temperature. These results suggest that the particular technique used to grow the present thin films (see Experimental Details in the Supporting Information) significantly affects molecular alignment and crystallinity. While the *d*-spacing values are comparable using sublimation and drop-casting for **NDI-1T**, they differ substantially for **PDI-3T** and **NDI-T-Ph-T**, where smaller *d*-spacings are found for solution processed vs sublimed films as shown in Figure 5. Nevertheless, for **NDI-T-Ph-T**, the *d*-spacing of the solution-processed films is comparable to that obtained for films grown at high sublimation temperatures (see Figure S2). Furthermore, a larger *d*-spacing is found for **PDI-1T** films.

Film Morphology by Atomic Force Microscopy. In this section, the surface morphology of the present semiconductor thin films is analyzed by AFM. Although this technique is unable to directly characterize the dielectric−semiconductor interface, AFM images are widely used to infer the microstructural properties of the charge transport active region in OTFTs.[52] Figure 7 shows AFM images of the present semiconductors deposited under the experimental conditions yielding optimal TFT performance. The AFM images of **NDI-1T** thin films deposited at 110 °C on HMDS-treated and OTS-treated substrates reveal polycrystalline surfaces with large planar terraces (∼1−2 μm) similar to, but larger than, those reported for other fused-ring semiconductors.[53] These terraces are more pronounced when the substrates are functionalized with HMDS. Even if the exact functional relationship between measured film mobility and grain size is still under active discussion,[54,55] a large number of reports have convincingly correlated the

(52) (a) Kim, P.; Zhang, X.-H.; Domercq, B.; Jones, S. C.; Hotchkiss, P. J.; Marder, S. R.; Kippelen, B.; Perry, J. W. *Appl. Phys. Lett.* **2008**, *93*, 013302. (b) Huang, T.-S.; Su, Y.-K.; Wang, P.-C. *Appl. Phys. Lett.* **2007**, *91*, 092116. (c) Pyo, S.; Son, H.; Choi, K.-Y.; Yi, M. H.; Hong, S. K. *Appl. Phys. Lett.* **2005**, *86*, 133508. (d) Lee, J.; Kim, J. H.; Im, S. *J. Appl. Phys.* **2004**, *95*, 3733. (e) Park, S. Y.; Park, M.; Lee, H. H. *Appl. Phys. Lett.* **2004**, *85*, 2283.
(53) Izawa, T.; Miyazaki, E.; Takimiya, K. *Adv. Mater.* **2008**, *20*, 3388.
(54) (a) Veres, J.; Ogier, S.; Lloyd, G. *Chem. Mater.* **2004**, *16*, 4543. (b) Veres, J.; Ogier, S. D.; Leeming, S. W.; Cupertino, D. C.; Khaffaf, S. M. *Adv. Funct. Mater.* **2003**, *13*, 199.
(55) (a) Yokoyama, T.; Park, C. B.; Nagashio, K.; Kita, K.; Toriumi, A. *Appl. Phys. Exp.* **2008**, *1*, 041801. (b) Park, Y. D.; Lim, J. A.; Lee, H. S.; Cho, K. *Mater. Today* **2007**, *10*, 46. (c) Kim, C.; Facchetti, A.; Marks, T. J. *Science* **2007**, *318*, 76. (d) Yagi, I.; Tsukagoshi, K.; Aoyagi, Y. *Appl. Phys. Lett.* **2005**, *86*, 103502. (e) Knipp, D.; Street, R. A.; Volkel, A.; Ho, A. *J. Appl. Phys.* **2003**, *93*, 347.

Table 4. OTFT Electrical Data for Vapor-Deposited Films of the Present Arylenediimide Semiconductor Series Measured in Vacuum and in Air on Si/SiO_2 Substrates[a]

			Vacuum			Air		
Semicond.	S^b	T_d (°C)	μ	V_T	I_{ON}/I_{OFF}	μ	V_T	I_{ON}/I_{OFF}
NDI-1T	H	110	0.35	28	10^6	0.10	50	10^7
	O	110	0.10	28	10^5	5×10^{-3}	50	10^5
	S	110	1.2×10^{-2}	55	10^2	–	–	–
NDI-3T	H	110	2×10^{-4}	10	10^2	5.5×10^{-5}	15	10^2
	H	25	3.5×10^{-4}	45	10^3	–	–	–
PDI-1T	H	110	0.15	27	10^7	0.08	42	6×10^7
PDI-3T	H	110	1.3×10^{-3}	45	10^4	1×10^{-4}	40	10^5
	O	110	3.5×10^{-3}	45	10^5	6×10^{-5}	40	10^4
NDI-T-Ph-T	H	25	7.4×10^{-2}	45	10^6	8×10^{-3}	40	10^7
	O	25	0.10	58	10^5	5×10^{-3}	57	10^6

[a] Electron carrier mobility (μ) is given in $cm^2\ V^{-1}\ s^{-1}$ and threshold voltages (V_T) in V. [b] Device parameters reported here are for films grown on untreated Si/SiO_2 substrates (S), hexamethyldisilazane vapor-treated Si/SiO_2 substrates (H), or octadecyltrichlorosilane-treated Si/SiO_2 substrates (O). Samples consistently exhibiting the best performance parameters are shown.

presence of large crystallite grains with enhanced mobility.[56] Furthermore, such planar terraces have been previously reported in a number of high mobility n-type oligothiophenes.[26] Both of the present **NDI-1T** films also exhibit crystal-like features protruding from the film surfaces, similar to those reported for N-fluoroalkyl perylenediimide derivatives.[13c]

Catenation of the thiophene core from one to three rings in **NDI-3T** markedly reduces the crystallite grain size, an observation usually attributed to the presence of a large density of grain boundaries and which is detrimental to electrical performance. The same effect, but less pronounced, is observed on replacing the naphthalenediimide unit with a perylenediimide group in **PDI-1T** and **PDI-3T**. Here, larger crystallites are detected compared to **NDI-3T** films, but not in comparison to **NDI-1T** films. Furthermore, in the case of **PDI-3T** films, larger grains are formed when this semiconductor is grown on OTS-treated substrates vs HMDS treatment. Finally, replacement of the central thiophene ring of **NDI-3T** by a phenylene group in **NDI-T-Ph-T** leads to a substantially increased grain size.

Field-Effect Transistor Characterization. Top-contact/bottom gate field-effect transistors were fabricated with vapor-deposited films of the present semiconductors to evaluate the charge transport characteristics via analysis of the OTFT current−voltage response. Performance parameters can then be extracted from the $I-V$ response plots within the assumptions of conventional transistor formalisms. These parameters include charge carrier mobility (μ), current on−off ratio (I_{ON}/I_{OFF}), and threshold voltage (V_T).[57] It is generally thought that, to be technologically viable, organic semiconductors must ideally exhibit mobilities of $\sim 0.1-1.0\ cm^2\ V^{-1}\ s^{-1}$, $V_T \approx 0.0$ V, and $I_{ON}/I_{OFF} \approx 10^6$ and must be environmentally stable.[5,58]

Table 4 summarizes the TFT performance data for the present semiconductors as vapor-deposited films. Transfer plots of I_D vs V_G were used to calculate the saturation mobility, threshold voltage, and current on−off ratio for all devices. To compare the electrical properties of the different semiconductors, the parameters were calculated for a $V_D = 100$ V. This voltage ensures that the device is operating in the saturation regime.

Device parameters are not reported for untreated substrates except for **NDI-1T** films since they generally exhibit an at least one order of magnitude lower mobility than films grown on SAM-functionalized substrates. These response differences can be ascribed to the presence of surface silanol groups on the SiO_2 dielectrics surfaces which are known to act as electron traps for materials having $E_{red1} < \sim -0.6$ V vs SCE.[6,59] The first reduction potentials of all the present semiconductor molecules are close to this value, which may explain the lower performance on untreated substrates. Nearly all of the present semiconductor films exhibit optimum device performance when deposited at relatively high temperatures (110 °C) and on SAM-treated-Si/SiO_2 substrates. Well-defined linear and saturation regimes are evident for all the materials in the output plots of I_D vs V_D for different gate biases (Figure 8).

The data in Table 3 indicate that the highest mobility for the present materials series is observed for vapor-deposited **NDI-1T** films grown at 110 °C on HMDS-treated substrates ($0.35\ cm^2\ V^{-1}\ s^{-1}$). This value is comparable to that reported for a perylene-diimide having *N*-octyl substituents, **PDI-8** (see chemical structure in Figure 1).[13c] Slightly lower mobilities ($0.1\ cm^2\ V^{-1}\ s^{-1}$) are found for **NDI-1T** films grown on OTS-treated substrates. **NDI-1T** films on bare Si/SiO_2 substrates yield devices with a somewhat lower electrical performance ($\mu_e = 1.2 \times 10^{-2}\ cm^2\ V^{-1}\ s^{-1}$), probably due to the aforementioned electron trapping by dielectric surface SiOH groups.[6] The insertion of an annelated oligothiophene fragment, yielding **NDI-3T**, greatly reduces the electron mobility, and only mobilities approaching 2.0×10^{-4} or $3.5 \times 10^{-4}\ cm^2\ V^{-1}\ s^{-1}$ can be obtained by growing the semiconductor at 110 or 25 °C, respectively, on HMDS-treated substrates. As noted above, sterically induced twisting of one of the **NDI-3T** thiophene rings from the molecular plane may interfere with close crystal packing, thus compromising intermolecular $\pi-\pi$ overlap. A similar effect was argued by Jones et al. for bromo- and chloro-substituted PDI derivates, **PDI-8Br2** and **PDI-8Cl4** (Figure 1), where substantial distortions from molecular planarity are observed and similar electron mobilities are measured ($10^{-5}-10^{-3}\ cm^2\ V^{-1}\ s^{-1}$).[13c] In the present case, the planarity of the arylene core is not affected; however distortion of the oligothiophene fragment is likely to similarly interfere with the crystal packing and $\pi-\pi$ overlap.

In **NDI-T-Ph-T**, substitution of the central thiophene ring by a phenylene fragment greatly enhances the electrical

(56) (a) Jeong, Y. T.; Dodabalapur, A. *Appl. Phys. Lett.* **2007**, *91*, 193509. (b) Kang, G.-W.; Park, K.-M.; Song, J.-H.; Lee, C. H.; Hwang, D. H. *Curr. Appl. Phys.* **2005**, *5*, 297. (c) Kim, Y.-M.; Pyo, S.-W.; Kim, J.-S.; Shim, J.-H.; Suh, C.-H.; Kim, Y.-K. *Opt. Mater.* **2002**, *21*, 425.

(57) Sze, S. M. *Semiconductor Devices*; John Wiley & Sons: New York, 1985; p 523.

(58) (a) Dodabalapur, A. *Nature* **2005**, *434*, 151. (b) Dimitrakopoulos, C. D.; Malenfant, P. R. L. *Adv. Mater.* **2002**, *14*, 99. (c) Bao, Z. *Adv. Mater.* **2000**, *12*, 227. (d) *Printer Organic and Molecular Electronics*; Kluwer Academic Publishers: New York, 2004; p 695.

(59) Yoon, M.-H.; Kim, C.; Facchetti, A.; Marks, T. J. *J. Am. Chem. Soc.* **2006**, *128*, 12851.

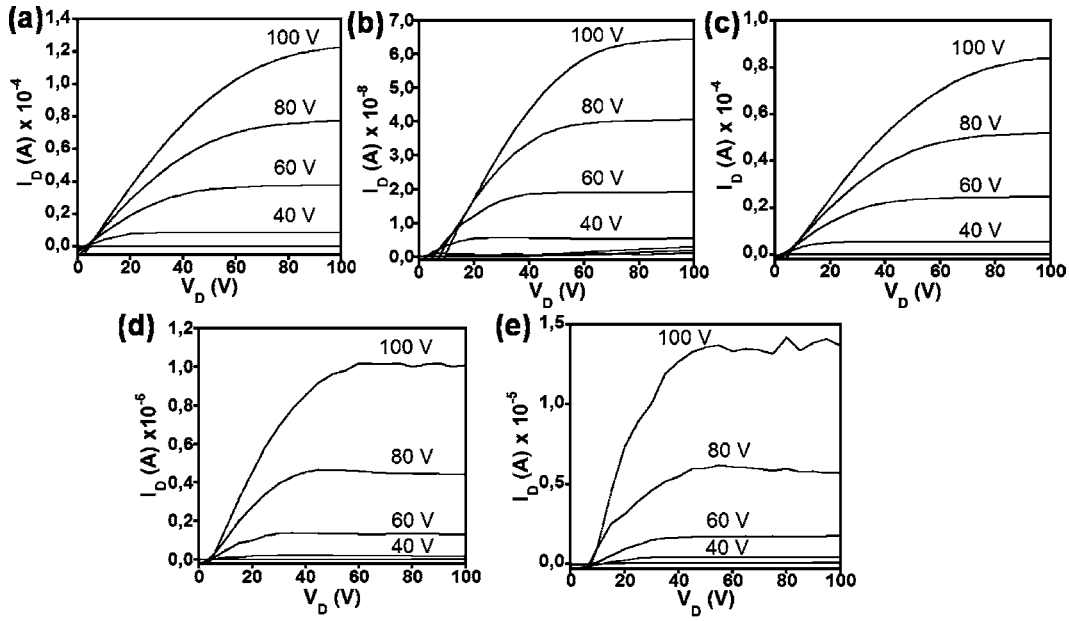

Figure 8. OTFT output characteristics of vapor-deposited (a) **NDI-1T**, (b) **NDI-3T**, (c) **PDI-1T**, (d) **PDI-3T** films grown at 110 °C on HMDS-treated Si/SiO_2 substrates and (e) **NDI-T-Ph-T** films deposited at 25 °C on OTS-treated Si/SiO_2 substrates.

performance, affording field-effect mobilities of 0.10 and 7.4 $\times$ 10^{-2} cm^2 V^{-1} s^{-1} for films grown at room temperature on OTS- and HMDS-treated Si/SiO_2 substrates, respectively. For **PDI-3T** films, substitution of the naphthalenediimide core (**NDI-3T**) by a perylenediimide core also enhances device performance but to a lesser extent, yielding devices with mobilities up to 1.3 $\times$ 10^{-3} and 3.5 $\times$ 10^{-3} cm^2 V^{-1} s^{-1} for HMDS and OTS-treated substrates, respectively. In marked contrast, the same substitution in **NDI-1T** leading to **PDI-1T** translates to a mobility decline by a factor of 2.

The threshold voltage[60] (V_T) refers to the gate bias (V_G) at which the carriers become mobile and is related to the voltage required to fill carrier trap states. The magnitude of this parameter is influenced by many factors, such as materials purity, atmosphere during device evaluation, substrate surface chemistry, semiconductor film morphology, film thickness, light exposure, etc.[61] The threshold voltage of all the present semiconductors varies between 27 and 45 V (Table 4). A lower V_T of $\sim$10 V is measured for **NDI-3T** films grown at 110 °C on HMDS-treated substrates.

Current on−off ratios are related to how efficiently the gate field modulates the "off" to "on" current, and a large "on" value is required for practical device applications. The highest I_{ON}/I_{OFF} here (10^7) is found for **PDI-1T** (Table 4). Following this, I_{ON}/I_{OFF} for **NDI-1T** deposited on HMDS- and OTS-treated substrates is 10^6 but falls to 10^2 when deposited on bare SiO_2 gate dielectrics. For **NDI-T-Ph-T** films, similar 10^5-10^6 values are observed. In the case of **PDI-3T**, I_{ON}/I_{OFF} is still substantial, 10^4-10^5, but declines for **NDI-3T** to 10^2-10^3. Such relatively low I_{ON}/I_{OFF} ratios are usually found in organic semiconductors having high electron affinities.[3,13a,28,62] The principal reason for the low I_{ON}/I_{OFF} in **NDI-3T** is the presence of a substantial current flow at $V_G = 0.0$ V of approximately 10^{-9} A. For the remainder of the present semiconductors, the "off" current is $\sim10^{-10}$ A for **NDI-1T** and **PDI-3T** and $\sim10^{-11}$ A for **NDI-T-Ph-T** and **PDI-1T**.

Figure 9 shows bidirectional transfer plots for all the present semiconductors, from which information about hysteresis can be extracted. The **NDI-1T**, **PDI-1T**, and **NDI-3T** semiconducting TFTs exhibit minimal hysteresis, while the **PDI-3T** and **NDI-T-Ph-T**-based devices exhibit significantly greater hysteresis, indicative of higher charge trap densities.

All TFT characterization measurements performed in vacuum were also performed in ambient atmosphere after breaking vacuum. As shown in Table 4, for all of the present semiconductors, mobility is degraded $\sim10\times$ upon air exposure. Moreover, the threshold voltages greatly increase ($\sim$20 V) in the case of **NDI-1T** and **PDI-1T**. For the remainder of the semiconductors, V_T remains essentially constant, indicating that an ambient atmosphere does not immediately increase the trap density in the films. For **NDI-1T**, **NDI-T-Ph-T**, **PDI-1T**, and **PDI-3T** films on HMDS-treated substrates, the I_{ON}/I_{OFF} ratio is increased by $\sim10^1$ upon air exposure, likely reflecting trapping of a dopant-induced charge which would otherwise increase I_{OFF}. The low value of I_{ON}/I_{OFF} for **NDI-3T** and its insensitivity to ambient reflect the high level of trap densities in vacuum, which remain almost unaltered upon exposure to air.

Solution-Processed Films. Finally, to demonstrate the feasibility of low-cost arylenediimide oligothiophene OTFT fabrication, top-contact bottom-gate solution-processed devices were also fabricated. For **NDI-1T**, dichloromethane was selected as the solvent, due to the low solubility of **NDI-1T** in chlorobenzene, which was used for the remainder of the semiconductors. Figure S3 shows the output characteristics of the solution-processed devices measured under vacuum, and Table 5 summarizes their

(60) Boudinet, D.; Le Blevennec, G.; Serbutoviez, C.; Verilhac, J.-M.; Yan, H.; Horowitz, G. *J. Appl. Phys.* **2009**, *105*, 084510.

(61) (a) Pernstich, K. P.; Haas, S.; Oberhoff, D.; Goldmann, C.; Gundlach, D. J.; Batlogg, B.; Rashid, A. N.; Schitter, G. *J. Appl. Phys.* **2004**, *96*, 6431. (b) Pernstich, K. P.; Goldmann, C.; Krellner, C.; Oberhoff, D.; Gundlach, D. J.; Batlogg, B. *Synth. Met.* **2004**, *146*, 325. (c) Horowitz, G.; Hajlaoui, R.; Bouchriha, H.; Bourguiga, R.; Hajlaoui, M. *Adv. Mater.* **1998**, *10*, 923.

(62) (a) Bao, Z.; Lovinger, A. J.; Brown, J. *J. Am. Chem. Soc.* **1998**, *120*, 207. (b) Laquindanum, J. G.; Katz, H. E.; Dodabalapur, A.; Lovinger, A. J. *J. Am. Chem. Soc.* **1996**, *118*, 11331.

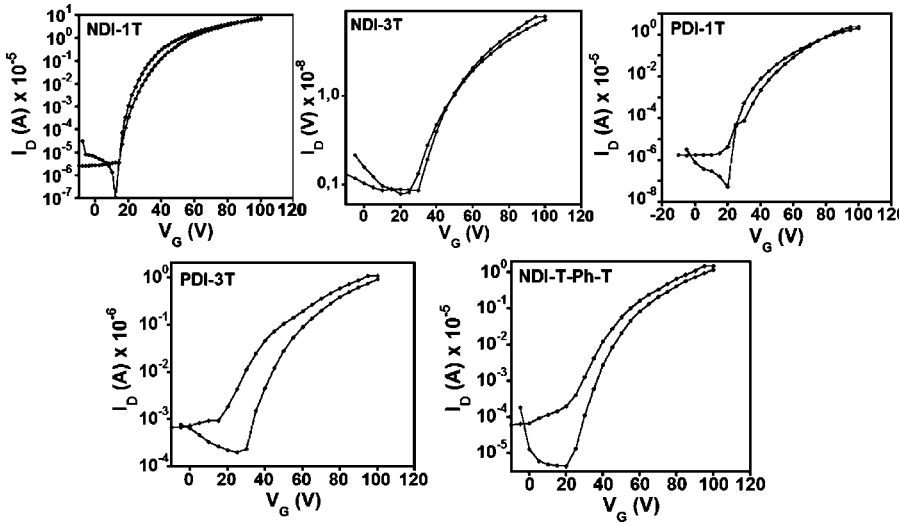

Figure 9. Bidirectional transfer plots for OTFTs fabricated from films of **NDI-1T** (T_d = 110 °C), **NDI-3T** (T_d = 110 °C), **PDI-3T** (T_d = 110 °C), **PDI-1T** (T_d = 110 °C), and **NDI-T-Ph-T** (T_d = 25 °C) grown on HMDS-treated Si/SiO_2 substrates by vapor techniques.

Table 5. Bottom-Gate Top-Contact (Unless Otherwise Specified) OTFT Electrical Data for Solution-Processed Films of the Present Arylenediimide Semiconductor Series Measured in Vacuum on HMDS-Treated Si/SiO_2 Substrates[a]

Semiconductor	μ	V_T	I_{ON}/I_{OFF}
NDI-1T	3×10^{-3}	33	10^{+5}
NDI-3T	4×10^{-5}	27	$2 \times 10^{+3}$
PDI-1T	0.042[b]	35	$5 \times 10^{+5}$
PDI-3T	4.5×10^{-3}	45	10^{+3}
	0.011[b]	50	10^{+3}
NDI-T-PH-T	8×10^{-4}	25	$3 \times 10^{+3}$

[a] Electron carrier mobility (μ) is given in $cm^2\ V^{-1}\ s^{-1}$, and threshold voltages (V_T) in V. [b] Top-gate bottom-contact OTFTs.

electrical performance. These plots reveal that, even from solution, the devices exhibit well-defined linear and saturation regimes, underscoring the structural quality of the semiconductor thin films. **PDI-3T** devices measured under vacuum exhibit an average mobility of $4.5 \times 10^{-3}\ cm^2\ V^{-1}\ s^{-1}$, a threshold voltage of ~45 V, and $I_{ON}/I_{OFF} \approx 10^3$; these parameters are comparable to those of the vapor-deposited films (Table 5). In contrast, for solution-processed **NDI-1T** and **NDI-T-Ph-T** films, the electron mobilities are lower by approximately 100× ($\mu = 3 \times 10^{-3}\ cm^2\ V^{-1}\ s^{-1}$ and $\mu = 8 \times 10^{-4}\ cm^2\ V^{-1}\ s^{-1}$, respectively) while the threshold voltage and I_{ON}/I_{OFF} are only slightly altered (V_T = 33 V and $I_{ON}/I_{OFF} = 10^5$) for **NDI-1T**. In the case of **NDI-T-Ph-T**, the threshold voltage falls to 25 V, and I_{ON}/I_{OFF} also falls to 3×10^3. **NDI-3T** films from solution also exhibit a lower performance compared to sublimed films, with a field effect mobility of $\mu = 4 \times 10^{-5}\ cm^2\ V^{-1}\ s^{-1}$, V_T = 27 V, and $I_{ON}/I_{OFF} = 2 \times 10^3$. In contrast to these top-contact OTFT results, a greater electrical performance is achieved using top-gate bottom-contact device geometries for **PDI-1T** ($\mu \approx 0.03\ cm^2\ V^{-1}\ s^{-1}$, $I_{ON}/I_{OFF} \approx 10^5$) and **PDI-3T** ($\mu \approx 0.007\ cm^2\ V^{-1}\ s^{-1}$, $I_{ON}/I_{OFF} \approx 10^3$) when measured under ambient conditions. The same samples were then measured under vacuum, and mobilities increased to 0.042 and 0.011 $cm^2\ V^{-1}\ s^{-1}$, respectively.

Discussion

Crystal Structure Analysis and DFT Semiconductor Molecular Structure Optimization. The optimized molecular geometries of all compounds under study were computed using DFT methods at the B3LYP/6-31G** level. Figure 10 shows that the naphthalene-thiophene core in **NDI-1T** is completely planar, while distortions are observed for the annelated oligothiophene molecules due to nonbonded repulsions involving the carbonyl group of the naphthalene/perylene cores, as seen above in the crystal structure of **NDI-T-Ph-T** (Figure 3). In this case, good agreement is found between the experimental metrical parameters and the theoretical calculations, as exemplified by the experimental and theoretical dihedral angles between the thiophene and aromatic planes: 64° vs 57°, respectively. The good accord between computed and experimental molecular structural results in **NDI-T-Ph-T** points out the accuracy of the DFT calculations for the present semiconductor series. For the remainder of the semiconductors, where single crystal diffraction data are not available, the theoretical dihedral angles are highlighted in Figure 10 and are essentially the same for **NDI-3T** and **PDI-3T** but differ from that of **NDI-Ph-T-Ph**. This distortion from planarity may be correlated with the lower observed crystallinity of the **NDI-3T** and **PDI-3T** thin films compared to those of **NDI-1T** and attendant lower carrier mobilities. Nevertheless, these angles are similar for the three molecules while crystal packing and electrical performance differ significantly. In particular, in **NDI-3T** and **NDI-T-Ph-T**, where only the central thiophene is replaced by a phenylene fragment, the vapor-deposited thin films are amorphous for the former material while some crystallinity is observed in the latter. For solution-cast films, where any sample thermal degradation on vaporization can be ruled out, higher crystallinity is observed for **NDI-T-Ph-T**. A computed parameter that helps in understanding this observation is the dipole moment, which greatly differs for these two molecules, 1.925 D for **NDI-3T** vs 0.7408 D for **NDI-T-Ph-T**, and which may stabilize different intermolecular stacking in the former. In fact, the calculated dipole moment for **NDI-3T** is even greater than that of **PDI-3T** (1.418 D), while that of **NDI-T-Ph-T** is similar to those of **NDI-1T** (0.618 D) and **PDI-1T** (0.503 D).

To correlate OTFT charge transport trends with molecular structural parameters, internal reorganization energies for electron transport were computed as previously described.[63] The intramolecular reorganization energy, λ, is a parameter that accounts for the structural reorganization needed to accom-

(63) Malagoli, M.; Bredas, J. L. *Chem. Phys. Lett.* **2000**, *327*, 13.

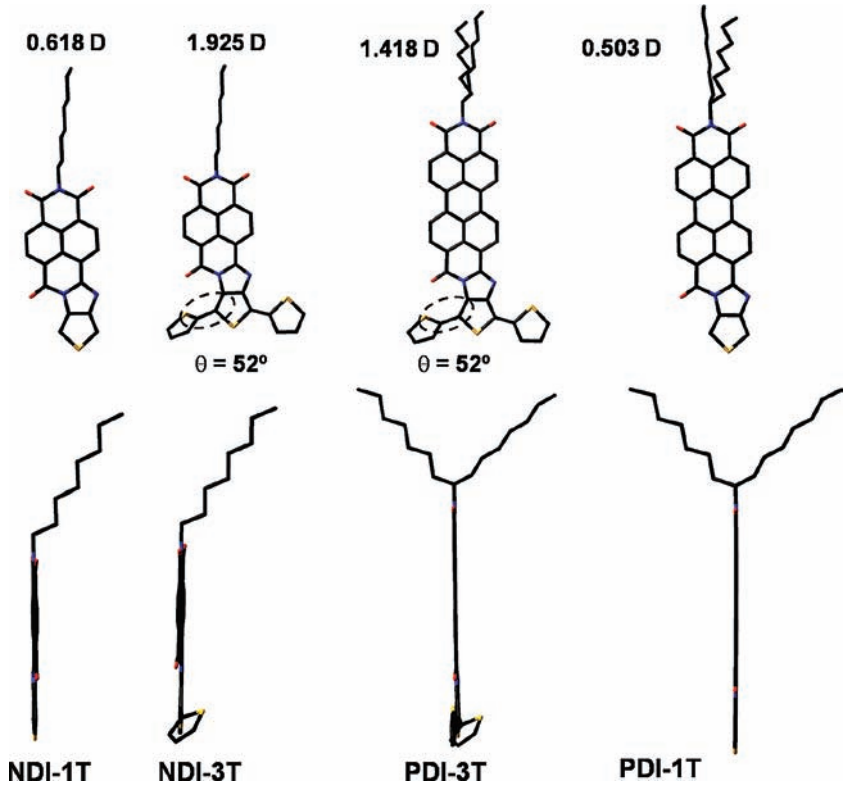

Figure 10. DFT//B3LYP/6-31G** geometry optimizations and computed dipole moments for the indicated semiconductors. θ gives the dihedral angle between the plane of the thiophene proximate to the carbonyl group and the arylenediimide core.

modate added charge as a prerequisite for efficient transport. The computed reorganization energies for the naphthalene derivatives are quite similar, 0.288 eV for **NDI-1T**, 0.298 eV for **NDI-3T**, and 0.300 eV for **NDI-T-Ph-T**. From these rather similar results, the differences in electrical performance are therefore most reasonably attributed to differences in film packing, order, and morphology. Lower λ values are estimated for perylene derivatives **PDI-3T** (0.221 eV) and **PDI-1T** (0.230). This result suggests that a logical strategy to further increase the **NDI-1T** field-effect mobility would be by substituting the naphthalene diimide core with a perylene diimide one, but using linear instead of the branched alkyl chains of **PDI-1T** which, as inferred from the XRD data, interfere with close crystal packing.

Carrier Mobilities of Vapor-Deposited OTFTs Measured in Vacuum. The differences in carrier mobilities between the four semiconductors of interest for vapor-deposited TFTs grown in vacuum can be understood on the basis of molecular packing and film microstructural trends. Indeed, superior device performance is measured for **NDI-1T** films, where calculations predict an essentially planar molecular structure. The absence of a significant distortion in the conjugated core promotes a closely packed, highly crystalline film with extensive Bragg progressions and a ~60° molecular tilt angle, favorable for efficient S→D charge transport. Furthermore, the film morphology assessed by AFM reveals the presence of large and well-connected grains, usually correlated with efficient charge transport.[52b,56]

The substitution of the naphthalenediimide fragment by a perylenediimide, in **PDI-1T**, translates to lower crystallinity (probably also reflecting the different alkyl chains) and smaller grain sizes, thus decreasing the mobility to 0.15 $cm^2\ V^{-1}\ s^{-1}$. Furthermore, the tilt angle here is significantly lower in **PDI-1T** (39.7°) vs **NDI-1T** (61.2°), which may impede charge transport.

In **NDI-Th-P-Th** films, the XRD data exhibit an elaborate diffraction pattern with the appearance of fourth-order Bragg reflections, while AFM indicates the presence of small, well-connected grains. The lower mobility of 0.1−0.074 $cm^2\ V^{-1}\ s^{-1}$ vs that of **NDI-1T** can thus be understood on the basis, among other factors, of the somewhat lower crystallinity (fourth order vs eighth order reflections for **NDI-1T**), a smaller molecular tilt angle (see Table 2), and the presence of smaller grains (~0.2 μm vs ~1−2 μm for **NDI-1T**). Smaller semiconductor grain sizes are expected to increase the density of grain boundaries, thereby increasing the threshold voltage by ~20−30 V.[64]

Carrier mobilities in **NDI-3T** OTFTs are significantly lower, $\sim 10^{-4}\ cm^2\ V^{-1}\ s^{-1}$, and are likely connected with the poor film crystallinity. Indeed, negligible diffraction is detected in XRD experiments for films grown at 110 °C. As noted in the previous section, this diminished crystallinity is likely related to the loss of molecular planarity caused by the thiophene annelation combined with the larger dipole moment which may disrupt packing, as well as the observed thermal degradation upon sublimation. The former factor may weaken $\pi-\pi$ overlap, which is also consistent with the lower melting point of **NDI-3T** vs **NDI-1T** (265 vs 280 °C). Furthermore, AFM images of **NDI-3T** films evidence very small grains with increased densities of

(64) (a) Kamins, T. I. *J. Appl. Phys.* **1971**, *42*, 4375. (b) Seto, J. Y. W. *J. Appl. Phys.* **1975**, *46*, 5247. (c) Baccarani, G.; Ricco, B.; Spadini, G. *J. Appl. Phys.* **1978**, *49*, 5565. (d) Levinson, J.; Shepherd, F. R.; Scanlon, P. J.; Westwood, W. D.; Este, G.; Rider, M. *J. Appl. Phys.* **1981**, *53*, 1193.

grain boundaries, which may impede charge transport.[65] In this semiconductor, it is interesting to note that similar mobilities are found for high and low temperature film growth, with only far higher threshold voltages (45 V vs 10 V) found for 25 °C growth devices. For 25 °C growth, the presence of very small grains creates charge trapping sites that must be filled prior to equilibrium device operation.[66]

The field-effect mobility of **PDI-3T** films is ~10× greater than that in **NDI-3T** films. Here, even if computation predicts a similar distortion of molecular planarity as in **NDI-3T** having a similar dipole moment, crystalline **PDI-3T** is observed in the XRD data. The higher mobility can be also ascribed to the increased grain sizes found in the AFM images vs **NDI-3T**. Furthermore, the grain sizes are found to be larger when the semiconductor films are grown on OTS-treated substrates, translating to slightly higher mobilities (1.3×10^{-3} cm^2 V^{-1} s^{-1} on HMDS-treated substrates vs 3.5×10^{-3} cm^2 V^{-1} s^{-1} on OTS-treated substrates).

In **NDI-3T** and **PDI-3T**, oligothiophene fragment annelation is proposed to induce ambipolar transport since the band gap is compressed vs **NDI-1T**, **PDI-1T**, and **NDI-Th-P-Th**. Previously, other groups showed that terthiophene functionalization with strong electron-withdrawing groups leads to smaller band gaps and to an ambipolar OTFT response.[27] In **NDI-3T** and **PDI-3T**, the absence of p-type behavior can be ascribed to the observed torsional distortion of the external thiophene ring, predicted by the computational analysis (*vide supra*). This distortion disrupts the oligothiophene π-conjugation, the only molecular characteristic likely to stabilize a positive charge. Thus, the distorted terthiophene fragment should behave largely as a bithiophene in terms of charge transport characteristics, and TFT activity has not been reported for the latter. Furthermore, head-to-tail crystal packing of these molecules would hinder proper HOMO overlap between the neighboring molecules, thereby impeding charge transport processes.

Effect of Ambient Environment on OTFT Performance. From the data in Table 3, a similar TFT mobility (~10×) is observed for all of the present semiconductors upon air exposure. This similarity can be understood by considering the similar electrochemical reduction potentials and, consequently, the similar electron affinities of all of these molecules. Furthermore, the first reduction potentials for these arylenediimide thiophene semiconductors are far from the −0.1 V metric considered to be the limit of organic semiconductor air stability.[13c] Nevertheless, despite the similar behavior upon air exposure, the temporal evolution of the electrical parameters under ambient differs substantially from semiconductor to semiconductor. Figure 11 shows the evolution of electron mobility and threshold voltage TFT with time exposure to air.

Note in Figure 11a that **PDI-3T** OTFTs degrade exponentially with exposure time in ambient, which translates into an approximately 10× lower mobility and higher threshold voltage within 90 days. In fact, threshold voltages as high as ~100 V are found after storage in air for ~90 days. Similar behavior is observed for **NDI-T-Ph-T** OTFTs while more rapid degradation is observed for **NDI-1T**. In marked contrast, the temporal response for **NDI-3T** is essentially unchanged for over 4 months in air, showing an essentially invariant electron mobility ($\sim 5 \times 10^{-5}$ cm^2 V^{-1} s^{-1}) and threshold voltage (~28 V). This result is surprising since **NDI-3T** exhibits the poorest film quality within the present semiconductor series as noted in the aforementioned XRD and AFM results. As discussed in previous sections, a different packing motif is expected for **NDI-3T** due to the large dipole moment, which may be the reason for the film air stability. The best performance under ambient conditions is found for **PDI-1T**, which combines good electrical behavior ($\mu \approx 0.06$ cm^2 V^{-1} s^{-1}) and air stability. Here, only slight mobility and threshold voltage changes are observed on ambient exposure.

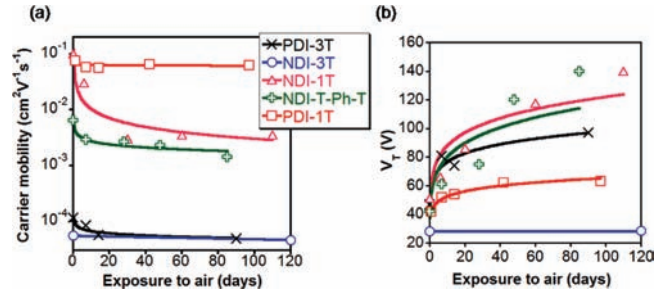

Figure 11. Time-dependent evolution in air of (a) TFT carrier mobility and (b) TFT threshold voltage of the indicated semiconductors. The semiconductors were deposited at 110 °C on HMDS-treated Si/SiO$_2$ substrates (25 °C in the case of **NDI-T-Ph-T**). The lines through the data points are drawn as a guide to the eye.

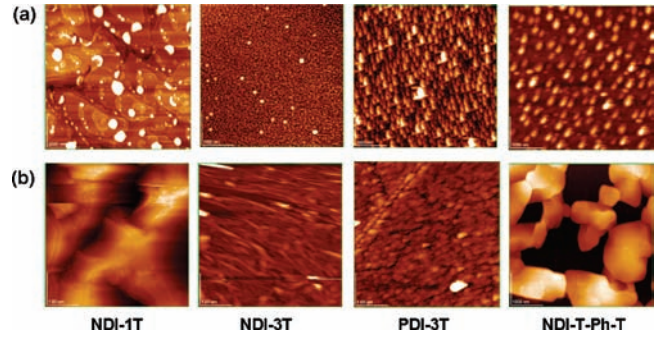

Figure 12. (a) AFM images of vapor-deposited films of **NDI-1T** (T_d = 110 °C on HMDS), **NDI-3T** (T_d = 25 °C on HMDS-treated Si/SiO$_2$ substrates), **PDI-3T** (T_d = 110 °C on HMDS), and **NDI-T-Ph-T** (T_d = 25 °C on OTS-treated Si/SiO$_2$ substrates). (b) AFM images of solution-processed films of the same materials.

Solution-Processed Field-Effect Transistors. The difference in electrical performance (bottom-gate top-contact devices) between films deposited by sublimation and from solution can be explained essentially in terms of film crystallinity and/or morphology. For example, for **PDI-3T** films, similar OTFT figures-of-merit are found using both deposition techniques (μ: 4.5×10^{-3} cm^2 V^{-1} s^{-1} for solution processing vs 3.5×10^{-3} cm^2 V^{-1} s^{-1} for vapor-deposited films). This result can be easily explained considering that similar film morphologies (grain size and shape) are obtained in both cases. Here, a high-boiling solvent was used and the substrates were heated at 60 °C, allowing the formation of well-connected grains. Note the presence of some degree of microstructural alignment from solution (Figure 12) that may enhance mobility. As indicated in Experimental Details in the Supporting Information, a pipet tip was used to spread the solution and obtain a homogeneous film, which may induce the aforementioned alignment. Furthermore, films from both solution and vapor deposition are

(65) Rivnay, J.; Jimison, L. H.; Northrup, J. E.; Toney, M. F.; Noriega, R.; Lu, S. F.; Marks, T. J.; Facchetti, A.; Salleo, A. *Nat. Mater.* **2009**, *8*, 952.

(66) (a) Weitz, R. T.; Amsharov, K.; Zschieschang, U.; Burghard, M.; Jansen, M.; Kelsch, M.; Rhamati, B.; van Aken, P. A.; Kern, K.; Klauk, H. *Chem. Mater.* **2009**, *21*, 4949. (b) Kelley, T. W.; Frisbie, C. D. *J. Phys. Chem. B* **2001**, *105*, 4538.

crystalline (see Figures 5 and 6), even if the *d*-spacing (and presumably orientation) changes from 30.2 to 25.0 Å, depending on the growth process.

XRD experiments on **NDI-1T** films, both solution-processed and vapor-deposited, yield essentially identical XRD data (see Figures 6 and 7), with a *d*-spacing of ~28.4 Å. These data together indicate that the lower field-effect mobilities from solution-processed films cannot be obviously ascribed to lower degrees of crystallinity. In contrast, comparison of the AFM images for both classes of **NDI-1T** thin films indicates very different film morphologies (Figure 12). In fact, the large planar terraces formed upon vacuum sublimation are not observed in solution growth, and large but poorly connected grains are found instead, which presages lower mobility.

In the case of **NDI-T-Ph-T** films deposited on HMDS-treated Si/SiO_2 substrates, lower OTFT performance is obtained from solution ($\mu \approx 8 \times 10^{-4}$ cm^2 V^{-1} s^{-1}) vs vapor-deposited films ($\mu \approx 7.4 \times 10^{-2}$ cm^2 V^{-1} s^{-1}), although greater sample crystallinity, with the appearance of fifth order Bragg reflections, is found in the solution-deposited films (see Figures 6 and 7). This can be understood considering that, for vapor growth at 25 °C, a larger *d*-spacing is observed, suggesting a larger molecular tilt angle or a different phase/growth orientation and, thus, enhanced field effect mobility. Note that identical *d*-spacings and diffraction features are found for solution- and vapor-phase film growth at higher deposition temperatures (see Figure S2), and consequently the mobilities are now similar (8×10^{-4} cm^2 V^{-1} s^{-1} from solution vs ~10^{-3} cm^2 V^{-1} s^{-1} for sublimed films grown at 90° or 110 °C on HMDS-treated Si/SiO_2). However, analysis of the solution-processed film morphology indicates the formation of larger grains, in good agreement with the decline in threshold voltage from 45 to 25 V, reflecting a decreased density of grain boundaries. For **NDI-3T**, solution processing leads to more crystalline films which however exhibit lower mobility (4×10^{-5} cm^2 V^{-1} s^{-1}). The AFM images shown in Figure 12 indicate a less homogeneous film which reasonably correlates with lower carrier mobility.

Finally, to improve the electrical characteristics of the solution-processed devices, top-gate bottom-contact OTFTs were fabricated with **PDI-1T** and **PDI-3T**, since these compounds offer the highest solubility. Polyera ActivInk D2200 was used as a dielectric layer. With these device architectures, electron mobilities are increased to 0.03 and 0.007 cm^2 V^{-1} s^{-1} for **PDI-1T** and **PDI-3T**, respectively, when measured in ambient and to 0.042 and 0.011 cm^2 V^{-1} s^{-1}, respectively, when measured under vacuum.

Conclusions

We have synthesized a new family of arylenediimide semiconductors for n-channel OTFTs, exhibiting field-effect mobilities as high as ~0.35 cm^2 V^{-1} s^{-1}, and compare/contrast their structural and electrical properties with a series of structurally related semiconductors. Specifically, OTFTs fabricated from **NDI-1T** films grown on HMDS-treated substrates at 110 °C exhibit the best electrical characteristics, with an electron mobility of 0.35 cm^2 V^{-1} s^{-1} and $I_{ON}/I_{OFF} = 10^6$ when measured under vacuum and 0.1 cm^2 V^{-1} s^{-1} upon air exposure. These device metrics erode with time and exposure to ambient. Lower mobilities, on the order of 0.15 to 10^{-4} cm^2 V^{-1} s^{-1} are recorded for the remainder of the semiconductor series. These variations in properties are analyzed by electrochemistry, thin-film XRD, and AFM, supported by DFT-level computation, leading to the following conclusions: (i) catenation of the oligothiophene backbone decreases the electrical performance due to skeletal distortions, while (ii) substitution of the naphthalenediimide fragment by a perylenediimide enhances the electron mobility when long oligothiophene skeletons, and thus molecular distortions, are present. This result can be ascribed to the greater film crystallinity and lower computed molecular reorganization energies of **PDI-3T** vs **NDI-3T**. An opposite effect is found for planar molecular structures; (iii) introduction of a phenylene group in the oligothiophene backbone enhances electron mobility via denser molecular packing.

Solution-processed top-contact bottom-gate OTFTs were also fabricated, and the electrical performance was compared to that of the corresponding vapor-deposited devices. Some performance improvement is found in **PDI-3T** TFTs by solution processing, which is ascribed to degradation upon sublimation and to the creation of partial grain alignment in the solution-based film growth technique, as shown in AFM images. Solution processed top-gate bottom-contact **PDI-1T** and **PDI-3T** devices exhibit air-stable electron mobilities of 0.030 and 0.007 cm^2 V^{-1} s^{-1}, respectively.

Acknowledgment. The research leading to these results has received funding from the European Community's Seventh Framework Programme under Grant Agreement 234808. We thank AFOSR (FA9550-08-01-0331), the NSF-MRSEC program through the Northwestern Materials Research Center (DMR-0520513) for support of this research at Northwestern University. We also thank Comunidad Autónoma de Madrid (Project S2009/MAT-1467), the UCM-BSCH joint project (GR58/08), and the MCyT of Spain (CTQ2007-60459) for financial support.

Supporting Information Available: Experimental and theoretical details, TGA plots, additional XRD data and CIF files. This material is available free of charge via the Internet at http://pubs.acs.org.

JA1018783